Supplement of the manuscript: "Agricultural flood risk under seasonally varying rainfall extremes and crop vulnerability"

Antonio Annis[1,2,3,4], Fernando Nardi[5], and Marco Marani[1,2]

[1]Department of Civil, Environmental and Architectural Engineering, University of Padua
[2]Research Center on Climate Change Impacts, University of Padova - Rovigo Campus
[3]Department of Geosciences, University of Padova
[4]Department of Land, Environment, Agriculture and Forestry, University of Padova
[5]Department of Civil Engineering and Computer Science Engineering, Tor Vergata University

Correspondence: Antonio Annis (antonio.annis@unipd.it)

This supplement provides additional figures and tables supporting the statistical, hydrological, hydraulic, and agricultural impact analyses presented in the main manuscript. Figures S1–S13 report diagnostic analyses related to the rainfall frequency framework, including the regional homogeneity assessment, marginal model evaluation, regional versus at-site configurations, return-level uncertainty, threshold sensitivity, and copula-based inter-duration dependence diagnostics. Figures S14-S18 provide additional information on the temporal structure of simulated rainfall events, intermittency properties, wet-fraction behaviour, selected observed hyetographs, crop phenological stages, and crop-specific depth-duration damage functions. These materials support the interpretation of the rainfall disaggregation procedure and the agricultural vulnerability component of the proposed framework.

Figures S19-S21 present supplementary crop-risk results, including duration-envelope expected annual losses by crop and hyetograph percentile, and expected annual production losses by crop, rainfall duration, and percentile. Tables S1-S3 provide additional statistical diagnostics and return-period ranges supporting the rainfall regionalization and copula-based design storm generation.

1 Supplementary figures

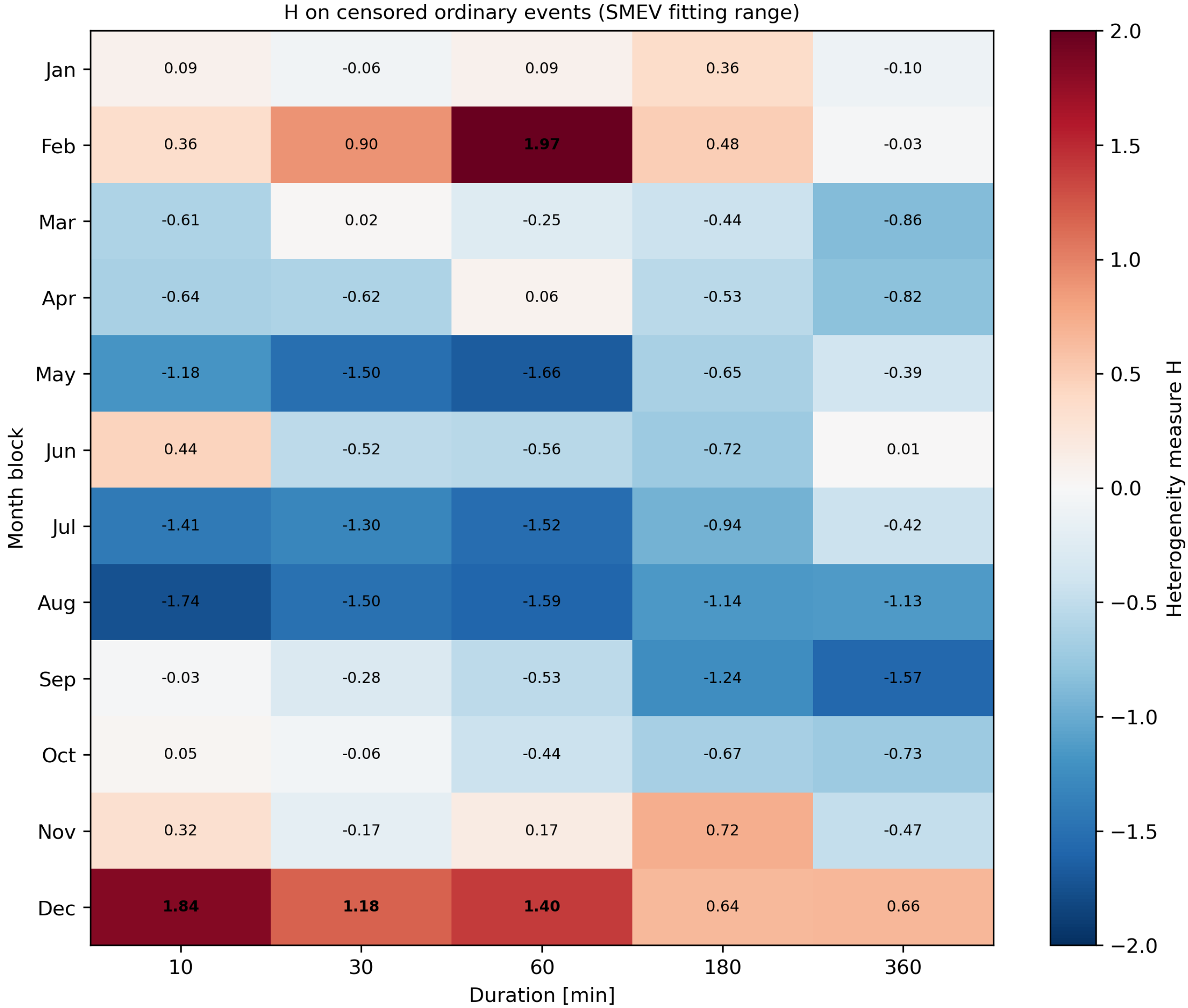

Figure S1. Heterogeneity measure H of the four rain gauges, for each month block (rows) and rainfall duration (columns). H computed on the left-censored ordinary events, i.e. on the portion of the event population to which the SMEV marginals are fitted; this is the quantity used to assess regional homogeneity. Values $H \geq 1$ are in bold. Under the Hosking–Wallis reading, $H < 1$ denotes an acceptably homogeneous region, $1 \leq H < 2$ a possibly heterogeneous one, and $H \geq 2$ a definitely heterogeneous one; negative values indicate gauges more similar to one another than repeated sampling from a common parent distribution would typically produce.

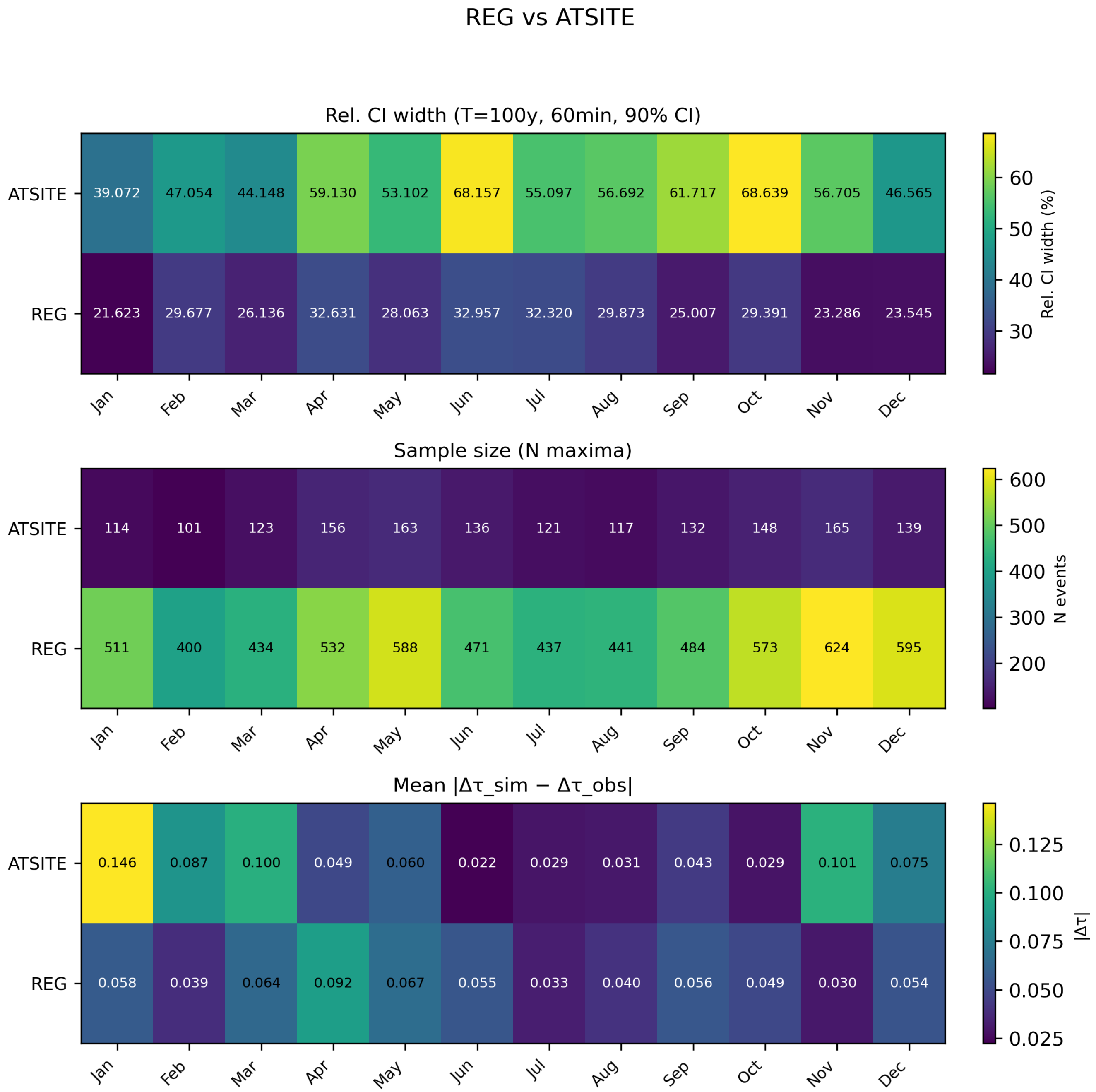

Figure S2. Confidence intervals widths with respect to the quantile values (upper panel), average sample sizes (central panel) and mean absolute difference between simulated and observed Kendall's coefficients (lower panel) for regional (REG) and at-site (ATSITE) configurations varying month

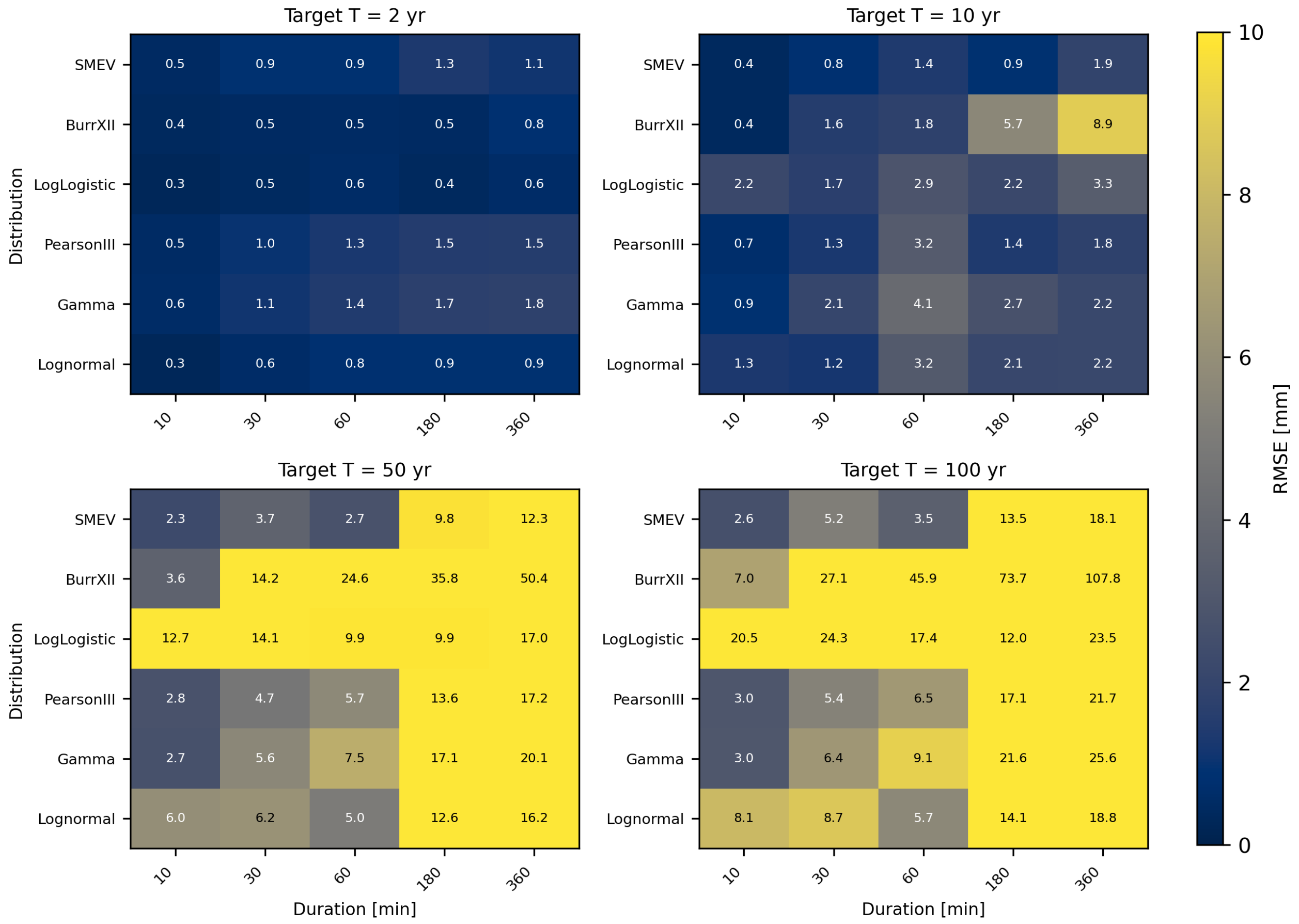

Figure S3. Heatmaps of the RMSE between empirical annual-maximum quantiles and those derived from fitted marginal models for selected durations and return periods.

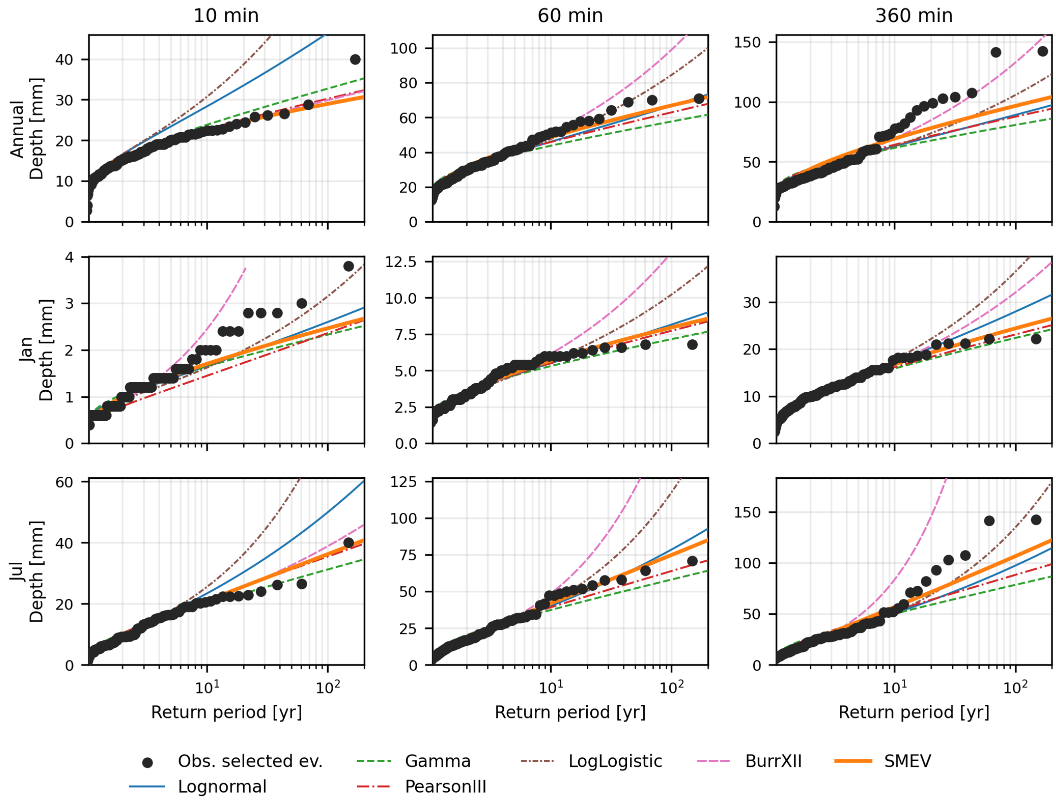

Figure S4. Return level curves from six candidate event-level distributions fitted to their respective calibration samples, compared against the empirical plotting positions of the observed events. Rows correspond to the annual sample, Januray and July; columns correspond to three aggregation durations. For all distributions except SMEV — Lognormal, Gamma, Pearson Type III, Log-Logistic, and Burr XII — the curves are fitted on the selected-event sample (events whose maximum accumulation exceeds the ≈1-year return level in at least one duration); the corresponding observed selected events are shown as dark circles, with their empirical return period on the horizontal axis. The SMEV distribution is fitted on the ordinary-event sample filtered at the event-level return period threshold $\rho_{\min}$ with left-censoring at the q-th empirical quantile. Annual-maximum return levels for all distributions are derived analytically via $F_{\mathrm{AM}}(x) = [F_{\mathrm{event}}(x)]^{\bar{n}}$, where $\bar{n}$ is the mean annual number of events in the respective calibration sample.

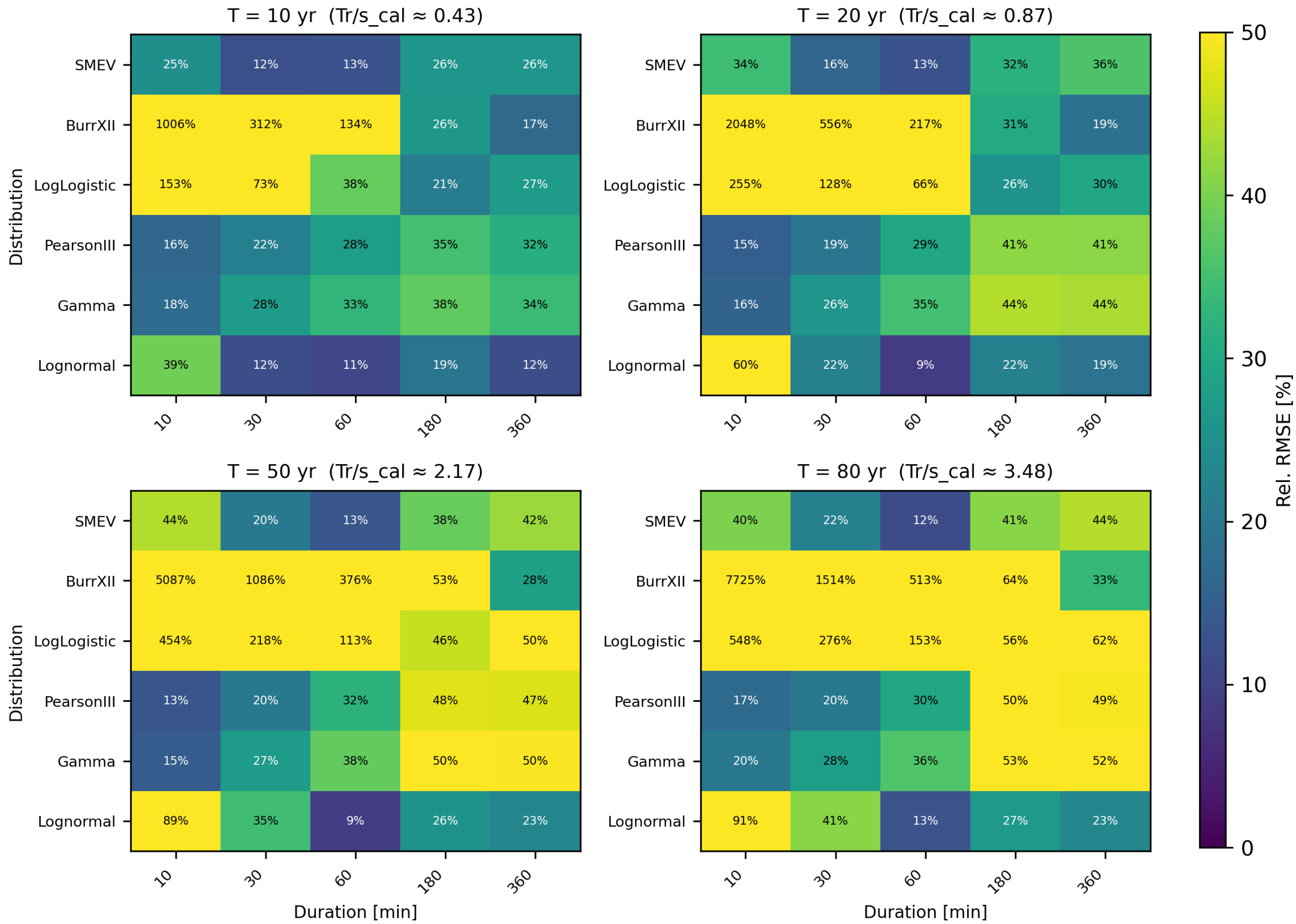

Figure S5. Cross-validated relative root mean square error (RMSE, %) of the T-year quantile estimated by seven candidate distributions, following a Monte Carlo approach. For each duration, the record is randomly partitioned into a $\sim$80% calibration set and a $\sim$20% validation set over 100 reshufflings. Each distribution is fitted on the calibration subset of its proper sample — selected events for Gamma, Lognormal, Pearson Type III, Weibull, Log-Logistic, and Burr XII; ordinary events filtered at $\rho_{\min}$ for SMEV — and evaluated against the empirical annual maxima of the corresponding validation subset using the Gringorten plotting position. Cell values are relative RMSE averaged over 100 Monte Carlo iterations and all months.

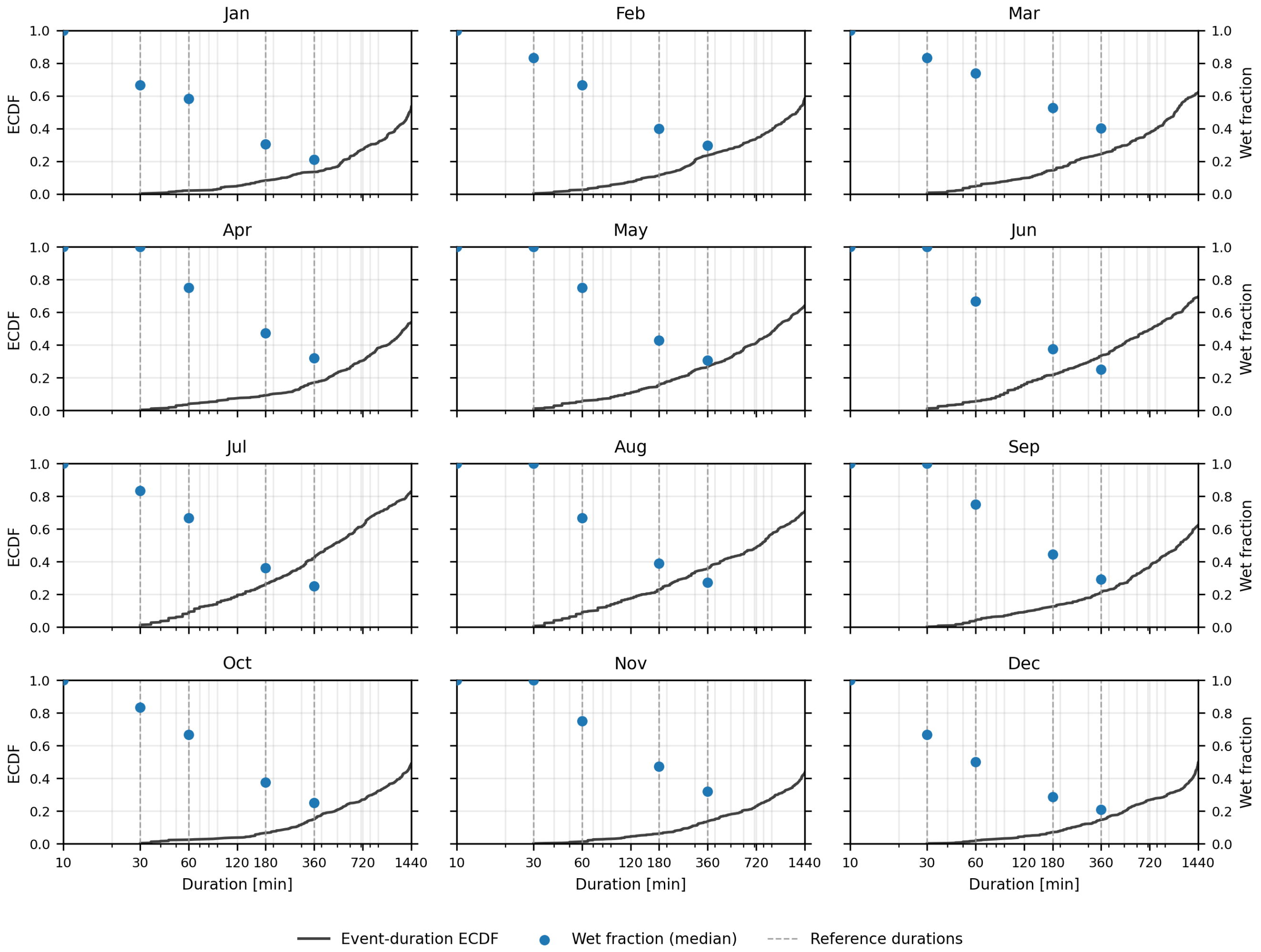

Figure S6. Empirical cumulative distribution function (ECDF) of observed event durations for a given month (solid line, left axis). Blue markers indicate the median wet fraction within the maximum rainfall window for the modelled durations (right axis). Vertical dashed lines denote the rainfall durations considered in the storm generator.

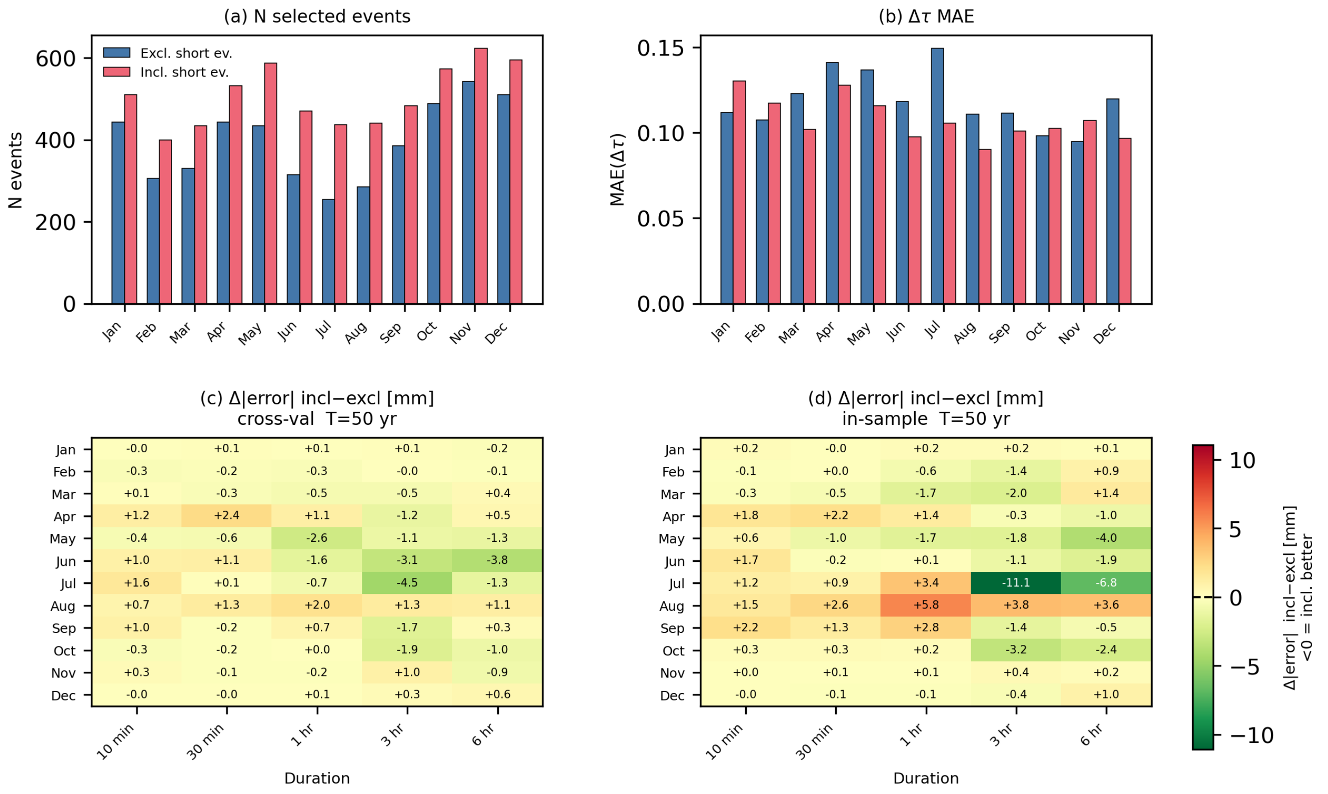

Figure S7. Effect of including short-duration events on the copula-based design storm model. Events shorter than the maximum design storm duration (360 min) are either excluded (blue) or zero-padded to 360 min and retained (red). For both configurations: (a) number of selected events per month; (b) mean absolute error of pairwise Kendall's τ differences ($\Delta\tau$) between observed events and unconditional samples from the fitted C-vine copula, computed over all duration pairs. Panels (c–d) show the difference of the RMSE of the 50-year return level between the two configurations (including/excluding short events); (c) Cross-validated RMSE ratio: years are randomly partitioned into 30% calibration and 70% validation sets over 100 Monte Carlo reshufflings; the marginal distribution is fitted on the calibration ordinary events and evaluated against the empirical annual maxima of the validation set. (d) In-sample RMSE diffrence: both configurations are fitted and evaluated on the full dataset. All marginal fits use the SMEV distribution.

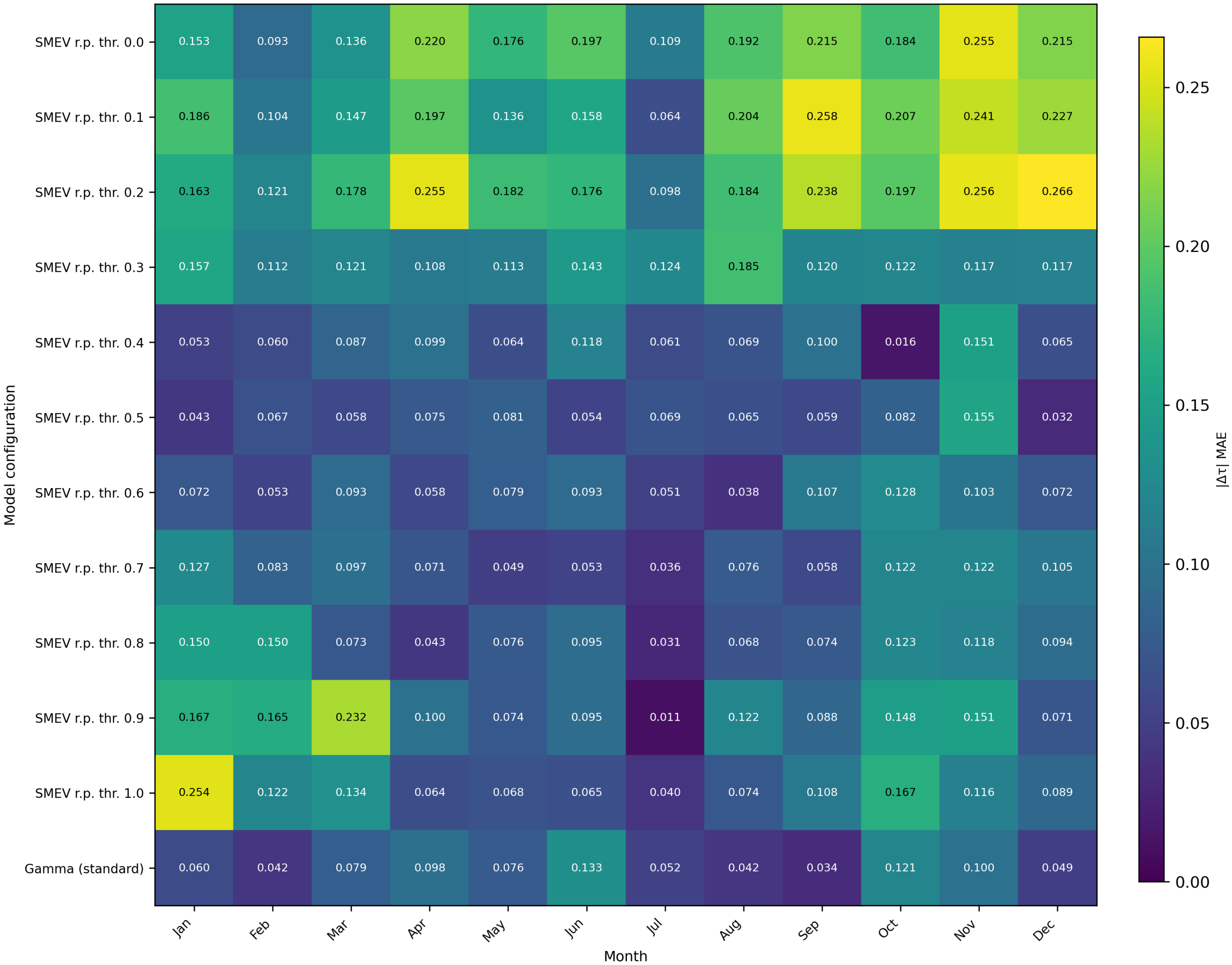

Figure S8. Mean absolute error of the pairwise Kendall's τ difference ($\Delta\ \tau$) between observed events and unconditional samples from the fitted C-vine copula for each month varying the returnn period as threshold for filtering the ordinary events used for the application of the SMEV distribution compared to the reference model **?** applying the Gamma distribution on the filtered extreme events caractherized by a return period higher than 1 year.

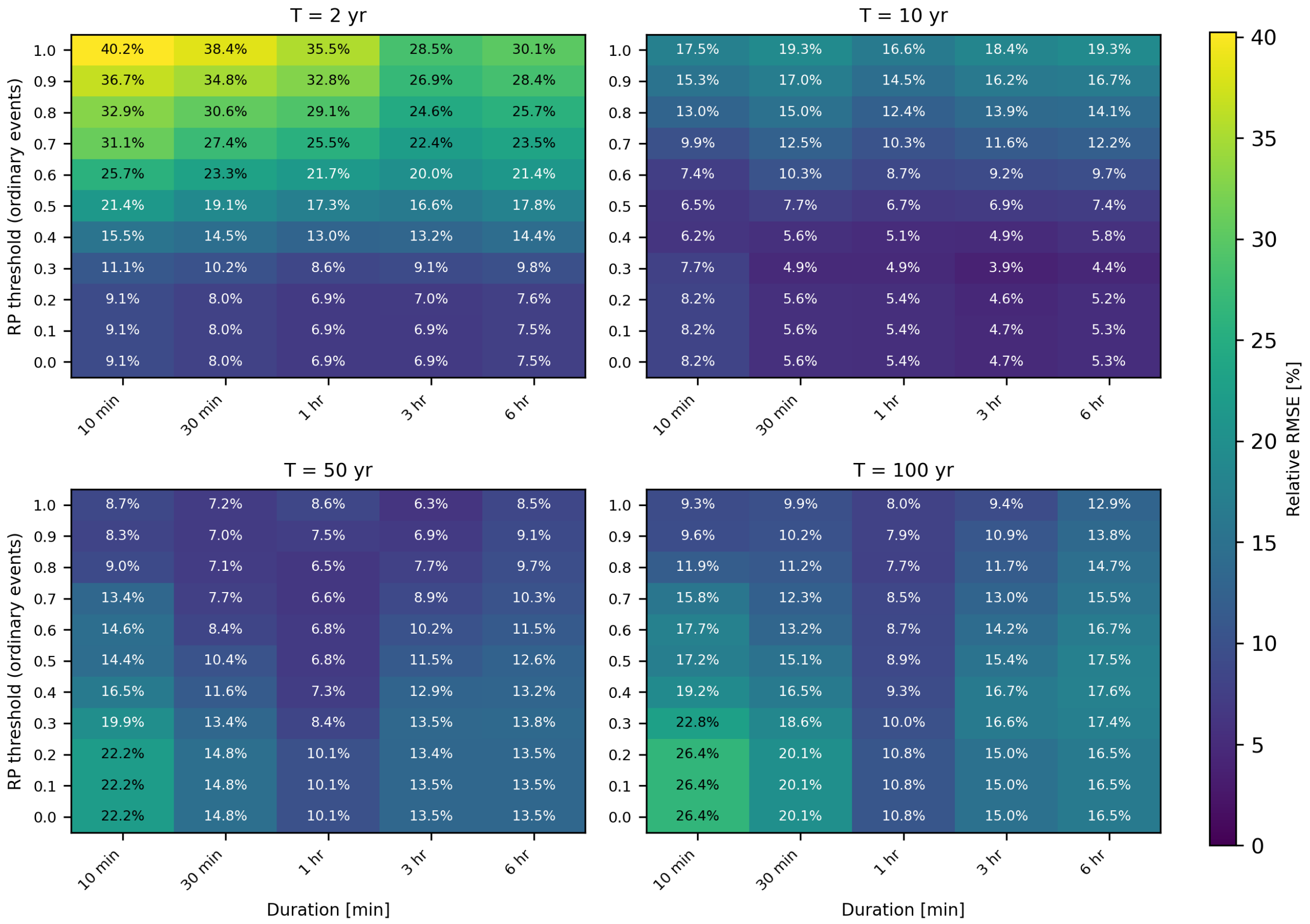

Figure S9. Root mean square error (RMSE, in %) of annual-maximum return levels from the fitted marginal distribution against empirical annual maxima averged over the months for different rainfall duration varying the ordinary-event filtering threshold for the SMEV-copula framework

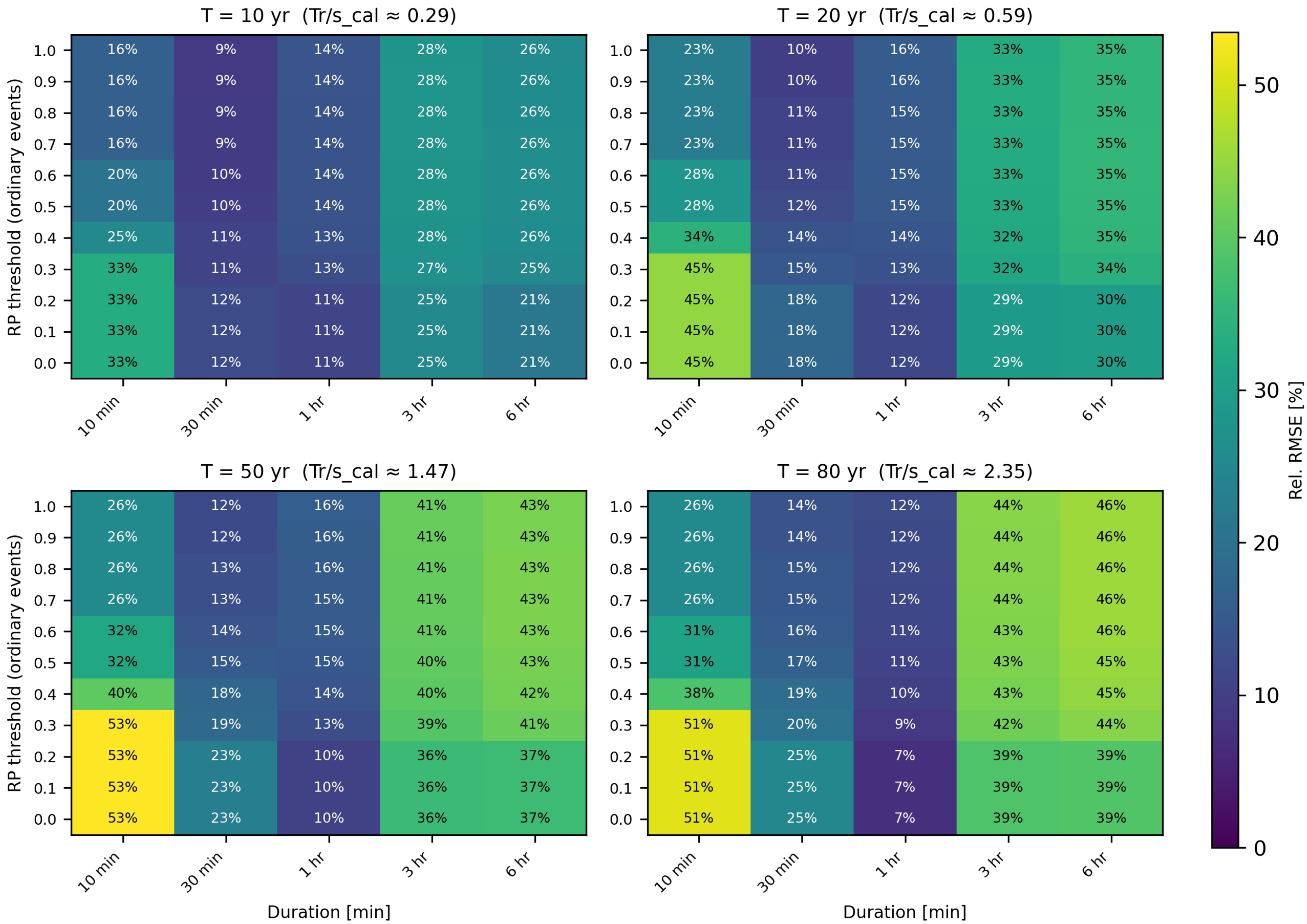

Figure S10. Root mean square error (RMSE, in %) of annual-maximum return levels as a results of a cross validation distribution against empirical annual maxima averged over the months for different rainfall duration varying the ordinary-event filtering threshold for the SMEV-copula framework

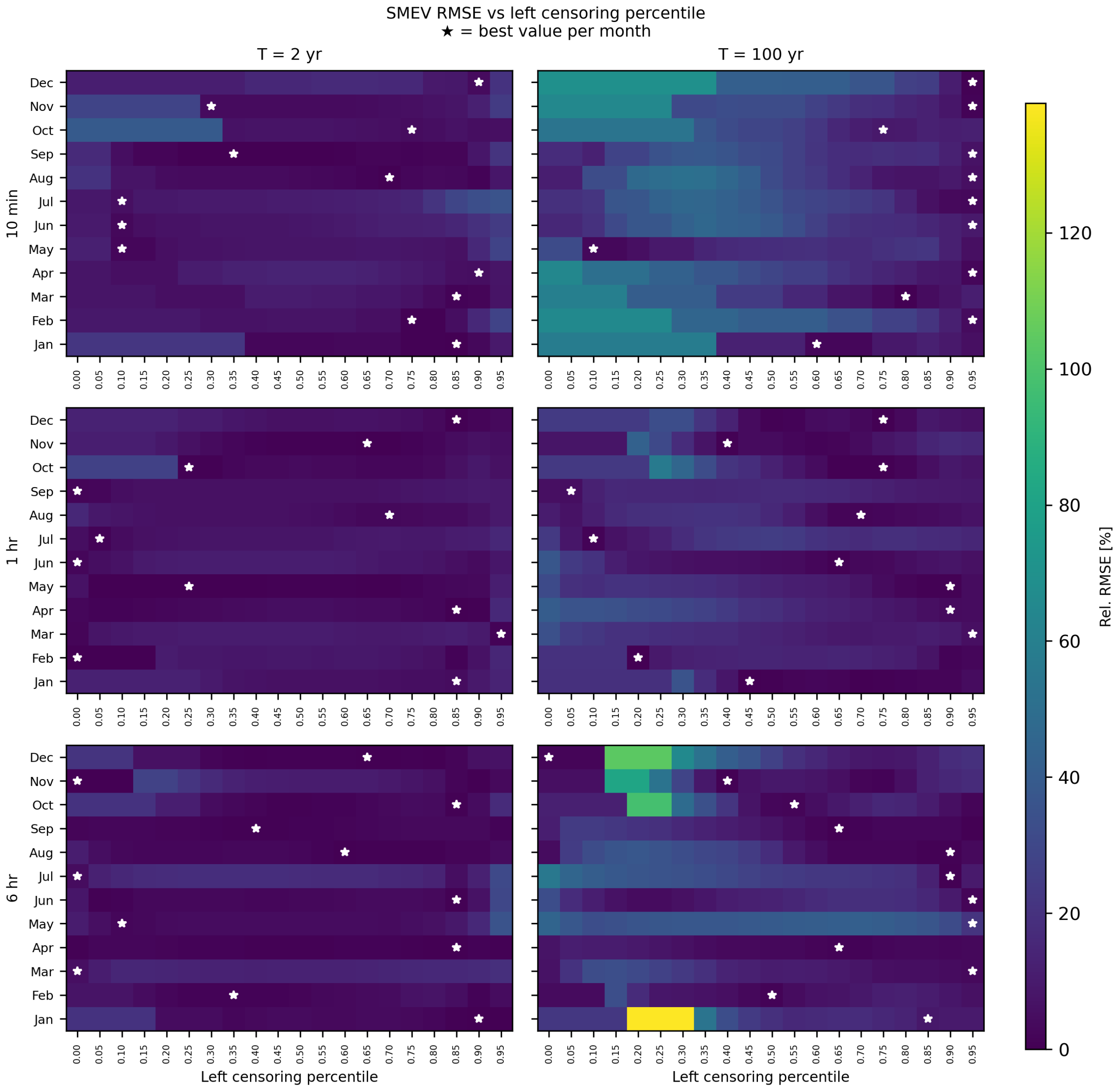

Figure S11. Root mean square error (RMSE, in %) of modelled quantiles against empirical quantiles for different rainfall durations (rows) and return periods (columns) varying the left censoring percentile

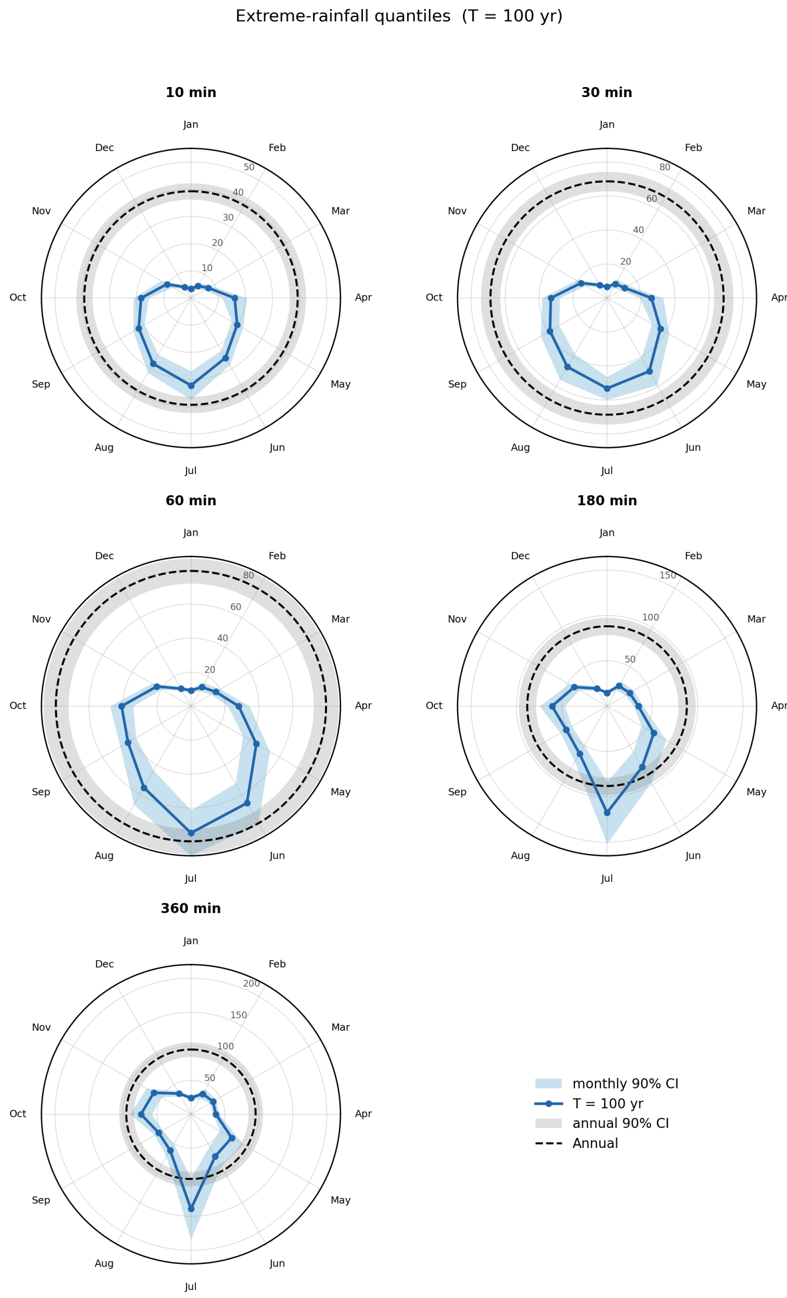

Figure S12. Radar representation of return level estimates at T=100 years across durations and months. Each axis corresponds to a duration, while values summarize the modelled quantiles and their associated uncertainty.

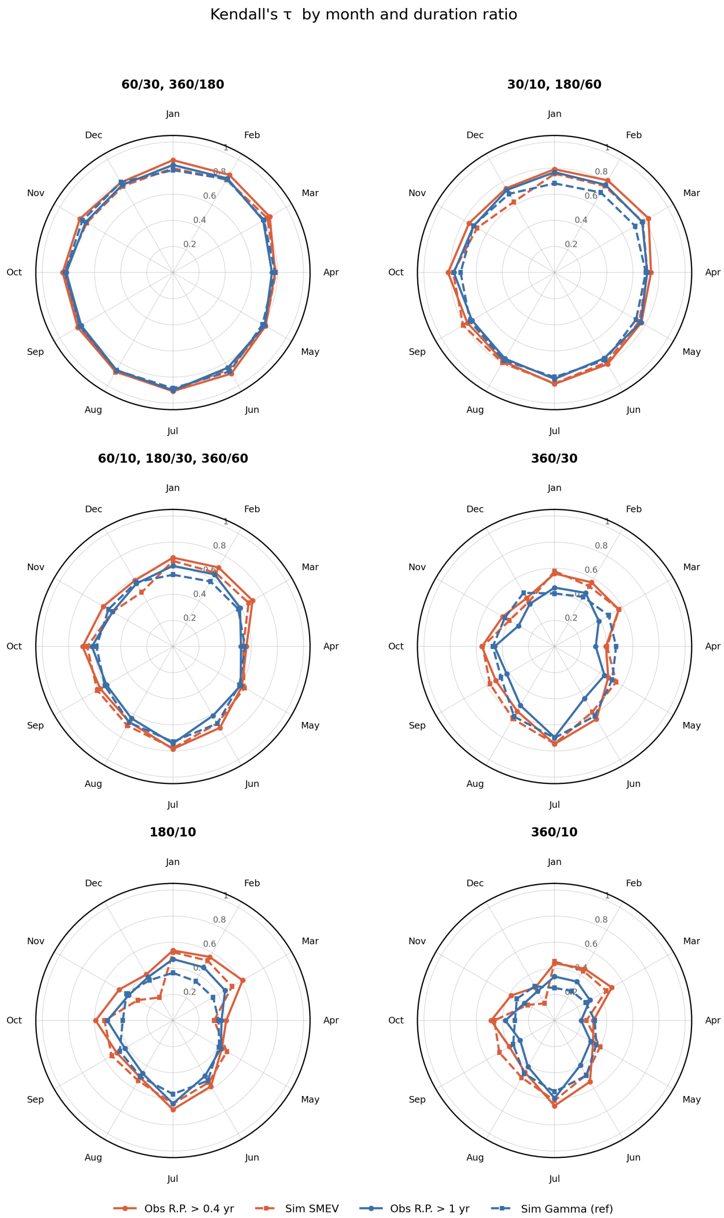

Figure S13. Radar representation of observed and simulated pairwise Kendall's τ as a function of duration ratio. Each panel shows four lines: observed τ computed on the selected-event sample used by the Gamma reference model (blue solid), unconditional copula simulation from the Gamma reference (blue dashed), observed τ computed on the ordinary-event sample used by the proposed SMEV model (orange solid), and unconditional copula simulation from the proposed SMEV model (orange dashed). The titles show the duration ratio d_j/d_i for all unique pairs (d_i, d_j) with $d_j > d_i$; values are averaged over pairs sharing the same ratio. The Gamma model uses the selected-event subset (return period exceeding $\approx$1 yr in at least one duration), while the proposed SMEV model uses the broader ordinary-event sample filtered at the event-level return period threshold $\rho_{\min}$.

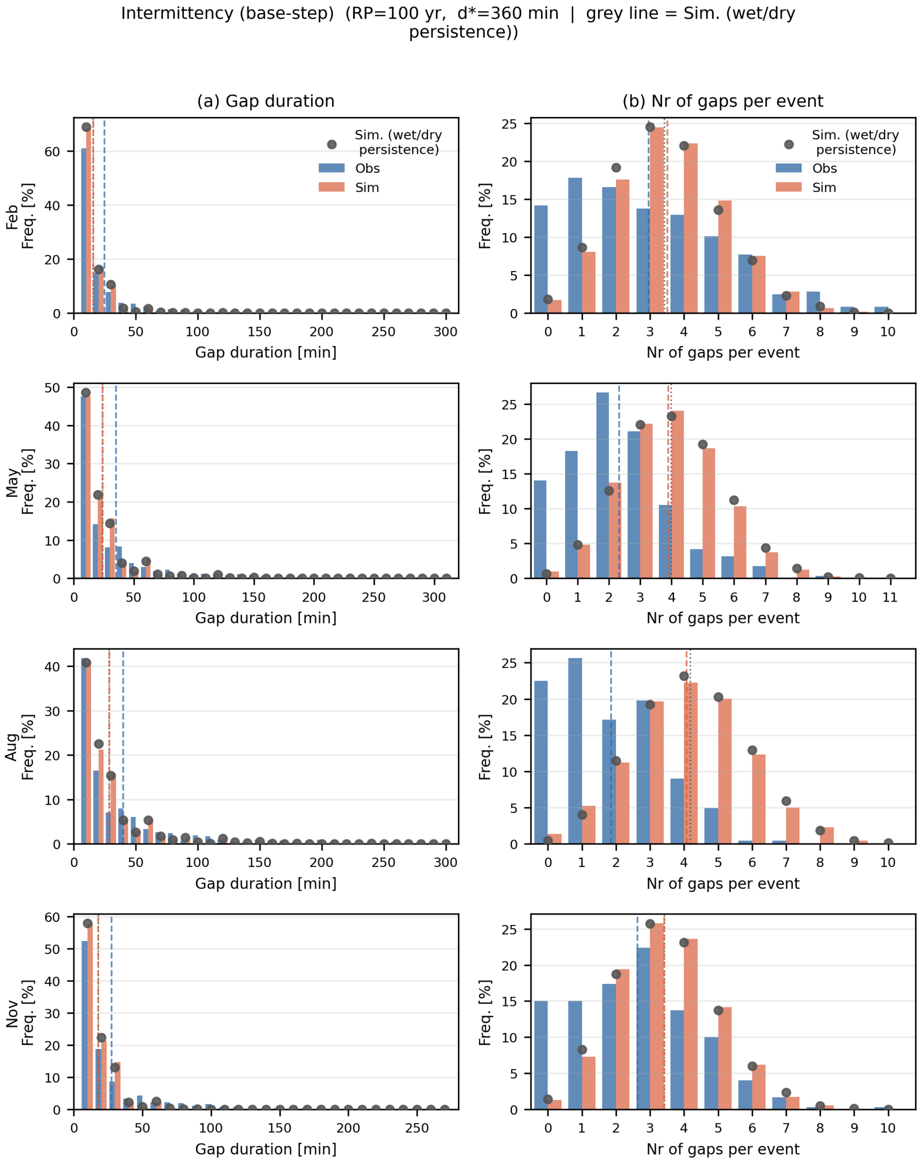

Figure S14. Intermittency characteristics of simulated hyetograph profiles (d*=360 min, T=100 yr) compared to observations, shown for four representative months. Left column: relative frequency distribution of dry-spell duration (in minutes at base time step resolution); right column: relative frequency distribution of the number of dry spells per event. Blue bars: observed; orange bars: simulated (current model). Grey dots: alternative model configuration with left-sibling wet/dry state conditioning (wet/dry persistence). A time step is classified as dry if rainfall intensity is below 0.2 mm per base time step. Vertical dotted lines mark the sample mean of each distribution.

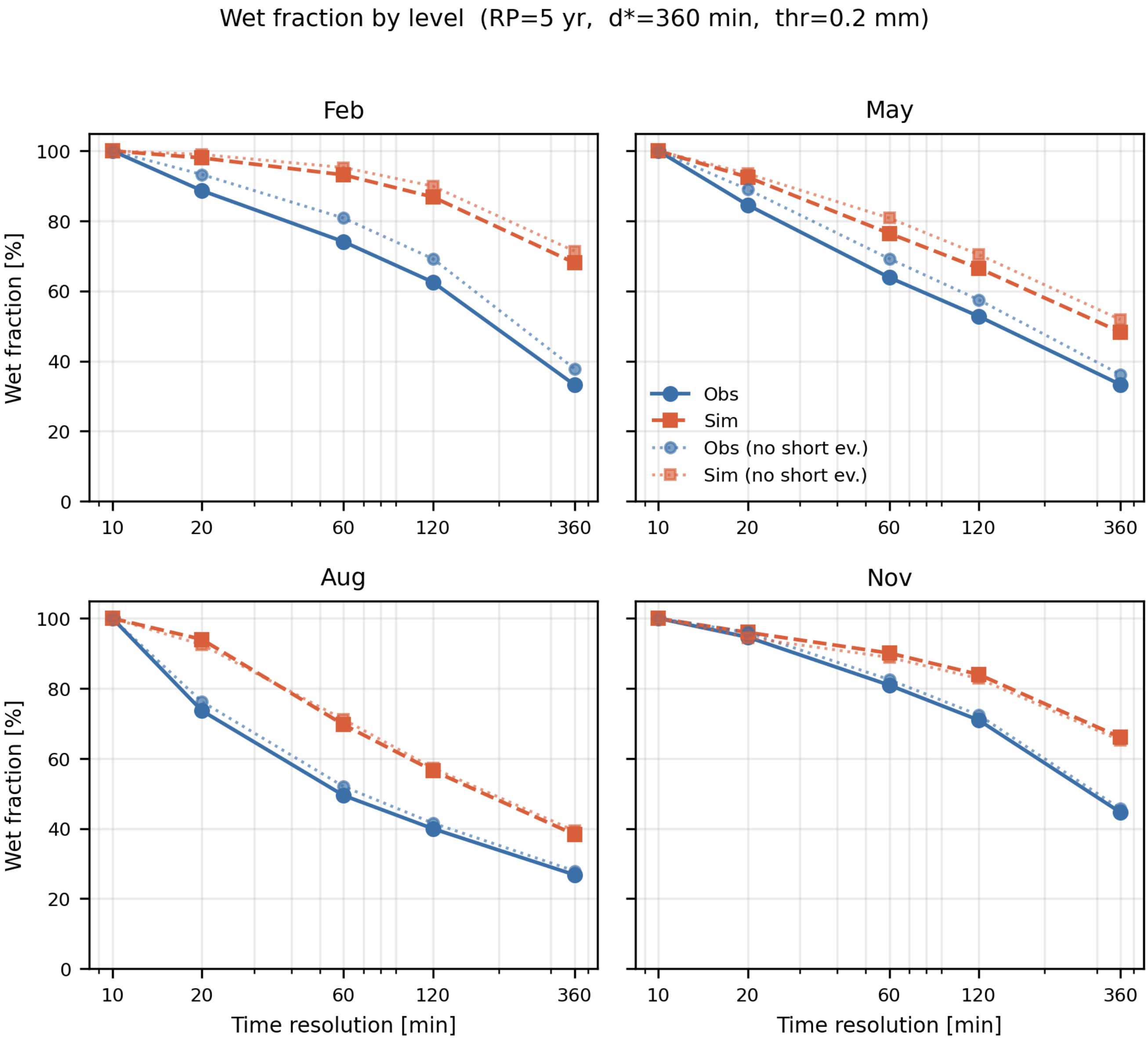

Figure S15. Wet fraction as a function of temporal resolution at each cascade disaggregation level, shown for four representative months (d*=360 min, T=5 yr, wet threshold =0.2 mm). Blue circles connected by solid lines: observed; orange squares connected by dashed lines: simulated. Lighter dotted lines of the same colours show the corresponding curves obtained when short-duration events are excluded from the calibration dataset.

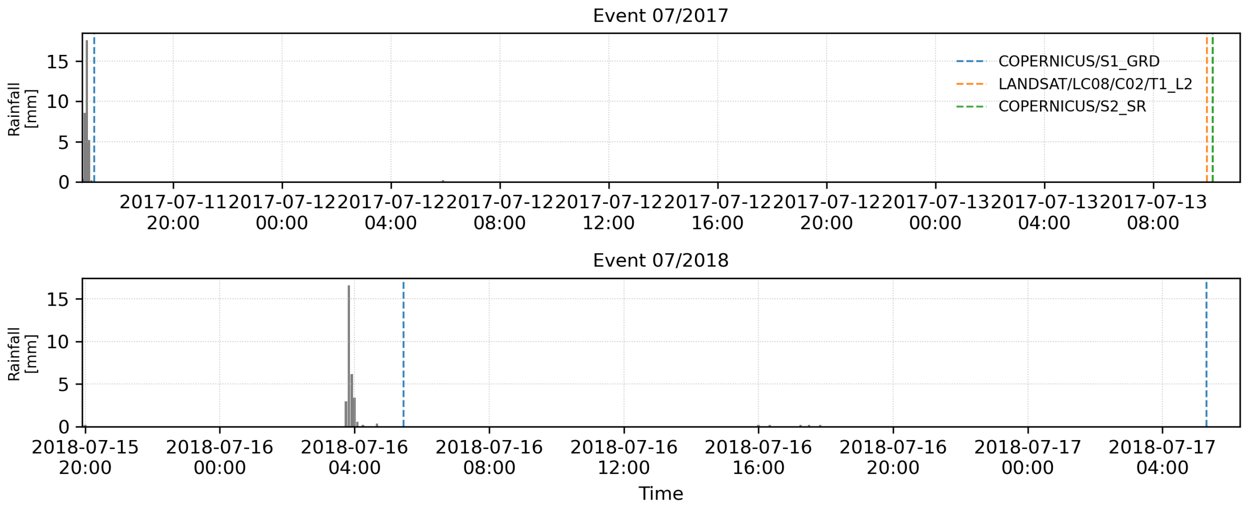

Figure S16. Hyetographs of the selected rainfall events (Events 07/2017 and 07/2018) with satellite overpass times. Rainfall is shown as bar plots, while dashed vertical lines indicate the acquisition times of available satellite images (Sentinel-1, Sentinel-2, and Landsat).

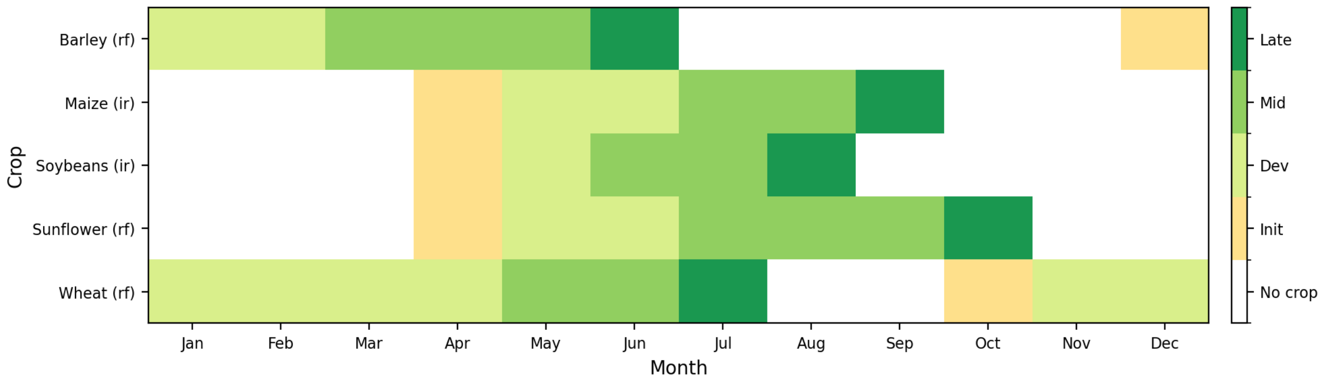

Figure S17. Crop stages for each month of the selected crops. Note that ir and rf stand for irrigated and rainfed.

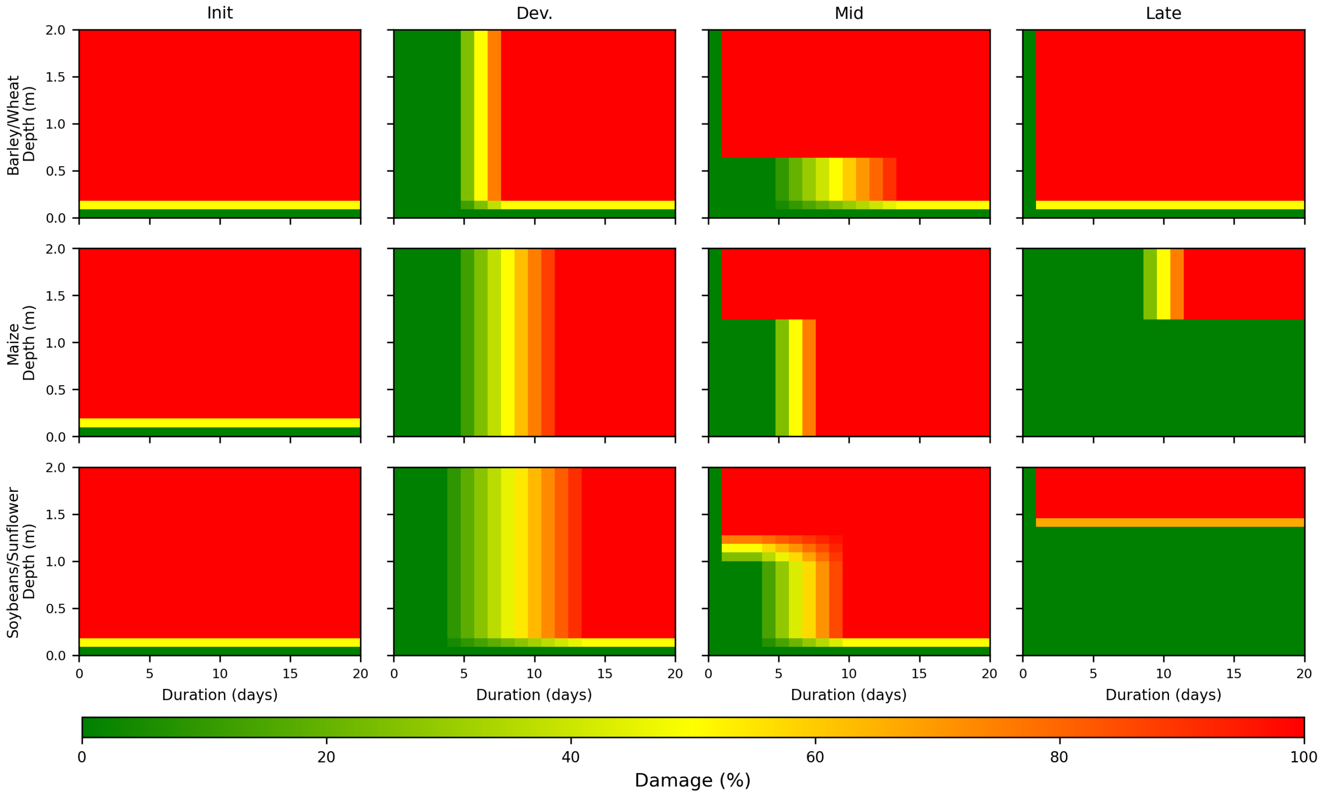

Figure S18. Damage curves of the selected crops as function of flow depths and duration

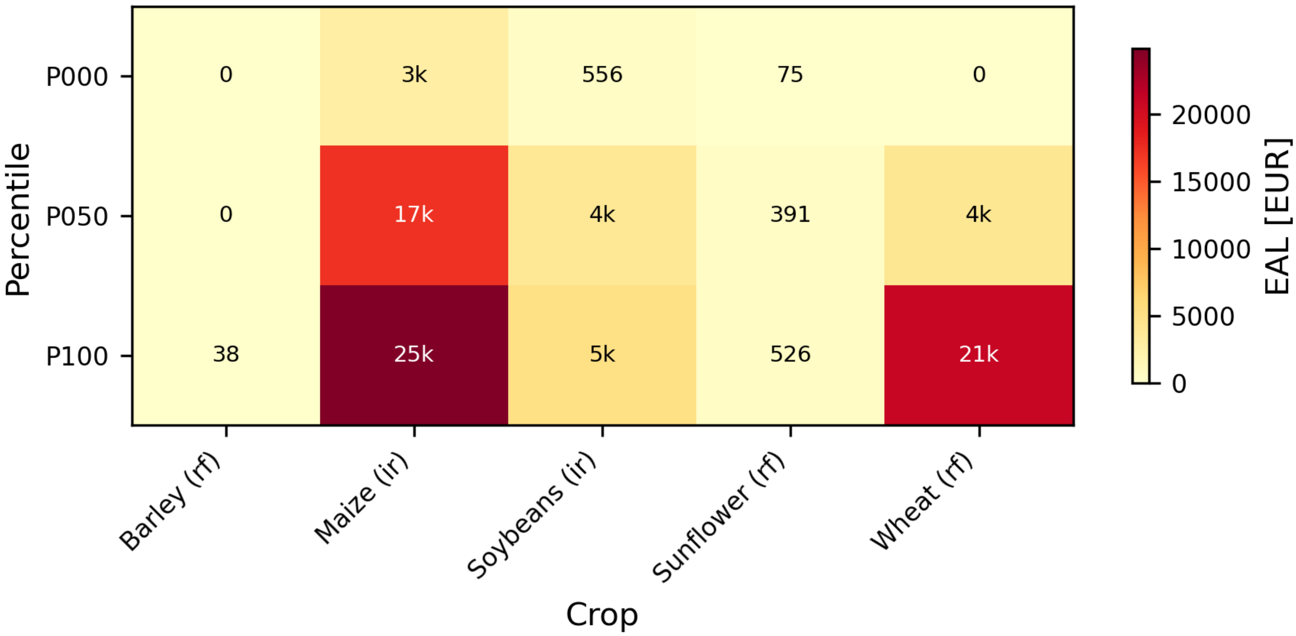

Figure S19. Heatmap of duration-envelope expected annual losses (EAL) for different crop types and hyetograph percentiles. Colors indicate the magnitude of aggregated economic losses (EUR)

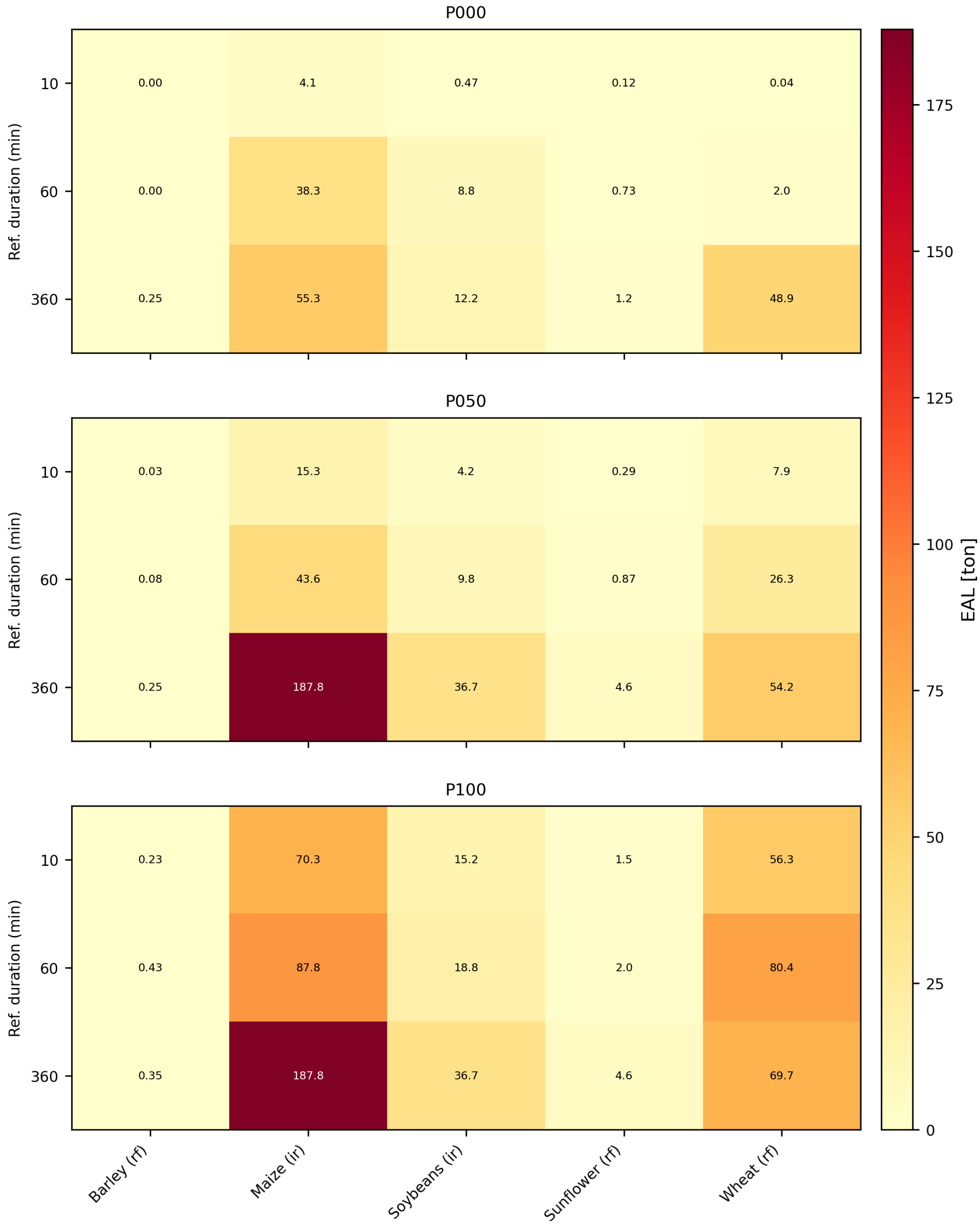

Figure S20. Heatmaps of expected annual losses (EAL) expressed in tons for different crop classes and rainfall durations under selected hyetograph percentiles. Each panel corresponds to a different percentile scenario

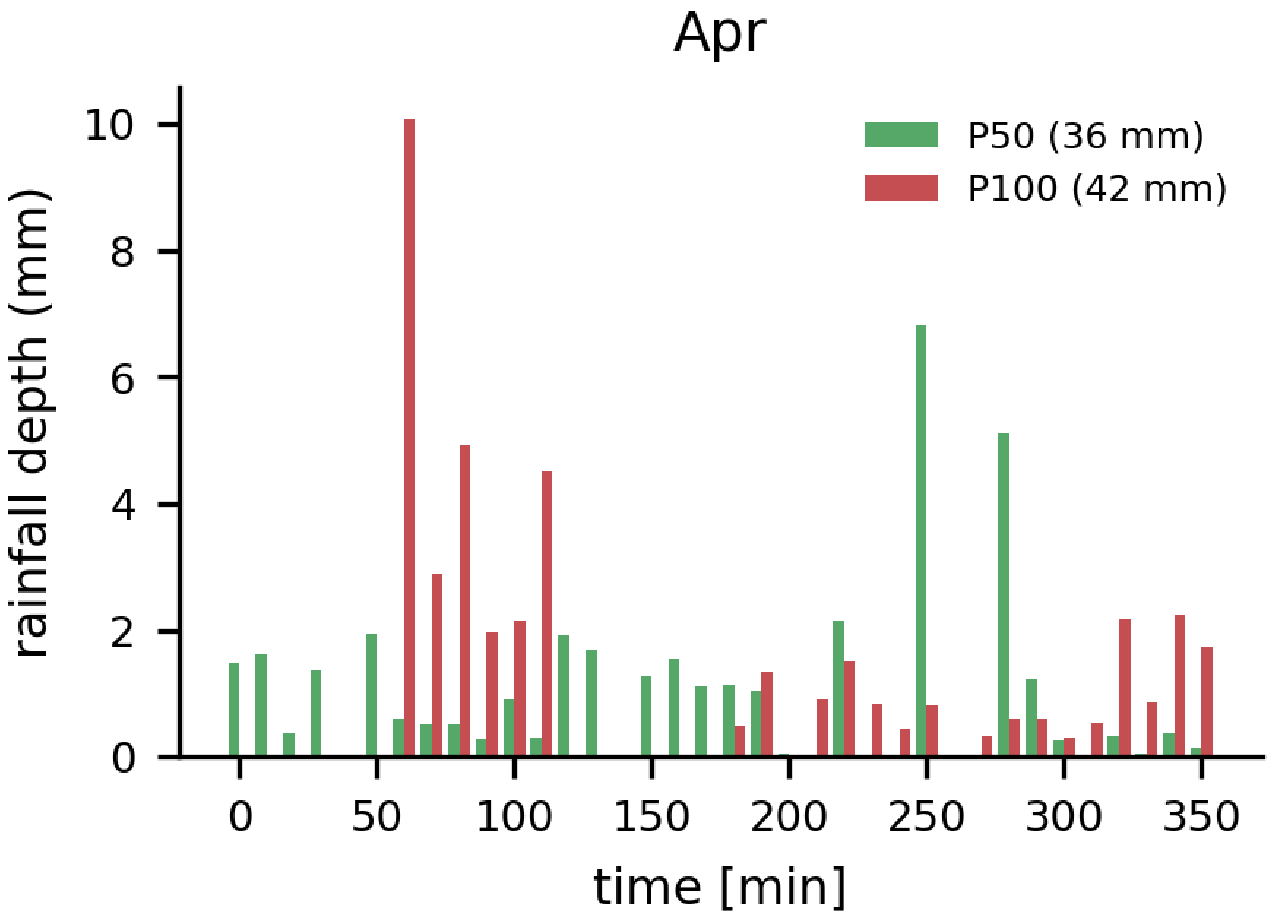

Figure S21. Synthetic hyetographs generated by the microcanonical model for a return period of 50 years and a reference duration of 360 min, for the 50th (P50, 36 mm) and 100th (P100, 42 mm) hyetograph percentiles, in April. Although P100 carries a larger total rainfall depth, its intensity is concentrated in an early single burst, whereas the peak intensities of P50 occur later in the event, acting on a soil already progressively wetted by the preceding rainfall. This difference in intra-event temporal structure explains why the lower-volume P50 hyetograph can produce a surface hydrological response, and hence a crop damage, comparable to that of the higher-volume P100 (cf. the near-equal EAL values at the 360 min duration for maize and sunflower in Figure S20).

2 Supplementary tables

Table S1. Regional homogeneity diagnostics for the ordinary events, by rainfall duration d. Range consider the 4gauges and the 12 month blocks. The regional Weibull shape parameter k and the heterogeneity measure H are estimated on the left-censored ordinary events (censoring percentile $q = 4$), i.e. on the portion of the distribution used by the SMEV marginal fit, and their range across month blocks is reported. $H < 1$ denotes an acceptably homogeneous region. KS refers to pairwise two-sample Kolmogorov–Smirnov tests on the censored tails, comparing every pair of gauges within each month block and duration (6 pairs per cell). The KS statistic D is the largest vertical distance between the two empirical cumulative distribution functions of a pair, so that a rejection indicates two gauges that cannot be regarded as samples of the same distribution. Rejections are counted twice: at the nominal significance level $\alpha = 0.05$, and at the Bonferroni-corrected level $\alpha/6$, which accounts for the fact that g pairs are tested within each cell and that testing several pairs inflates the probability of at least one spurious rejection. $D_{\max}$ is the largest D across all pairs and month blocks at a given duration; smaller values denote more similar gauges.

d (min)	Regional k	H	Blocks with $H < 1$	KS rejections ($\alpha = 0.05$ / Bonf.)	$D_{\max}$
10	0.73–0.98	-1.74 to $+1.84$	11/12	0 / 0	0.247
30	0.78–1.07	-1.50 to $+1.18$	11/12	1 / 0	0.276
60	0.78–1.18	-1.66 to $+1.97$	10/12	1 / 0	0.282
180	0.73–1.25	-1.24 to $+0.72$	12/12	0 / 0	0.246
360	0.71–1.25	-1.57 to $+0.66$	12/12	0 / 0	0.237

Table S2. At-site and regional Weibull shape parameter k estimated from the left-censored ordinary events at the 60 min duration, together with the heterogeneity measure H, by month block. Because the L-CV of a two-parameter Weibull depends on k alone, H is a test on the homogeneity of the shape parameter, i.e. of the tail behaviour extrapolated by SMEV. The seasonal gradient of k reflects the shift from heavy-tailed convective storms in summer to lighter-tailed stratiform precipitation in winter. At-site shapes agree closely in all month blocks except Feb and Dec (values of H in bold), where the residual spread reflects the winter low-tail artefact.

Month	Gauge				Regional	H
	98	121	151	152	k	
Jan	1.27	1.09	1.08	1.35	1.18	$+0.09$
Feb	1.56	0.99	0.94	1.27	1.13	$+1.97$
Mar	1.02	1.17	1.03	0.90	1.02	-0.25
Apr	1.06	0.95	0.95	0.82	0.95	$+0.06$
May	0.94	0.88	0.94	0.89	0.91	-1.66
Jun	0.73	0.82	0.91	0.80	0.80	-0.56
Jul	0.79	0.81	0.81	0.74	0.78	-1.52
Aug	0.93	0.99	0.94	0.99	0.96	-1.59
Sep	0.93	0.90	1.09	1.01	0.98	-0.53
Oct	0.92	0.79	0.85	0.93	0.87	-0.44
Nov	0.92	1.01	1.17	1.09	1.04	$+0.17$
Dec	1.27	1.13	0.89	1.11	1.07	$+1.40$

Table S3. Ranges of return periods of rainfall quantiles derived from copula-based simulations, for durations between 10 min and 6 h, conditioned on selected durations and reported for four representative months.

$T_{anc}[yr]$	d_{anc}	Feb	May	Aug	Nov
5	10 min	1.2 - 14.9	1.3 - 26.2	1.5 - 16.3	1.2 - 17.5
5	30 min	1.8 - 15.6	1.9 - 20.5	2.6 - 17.9	1.7 - 42.5
5	1 h	2.3 - 26.2	2.2 - 23.2	2.2 - 30.9	2.3 - 53.8
5	3 h	2.2 - 20.3	1.5 - 25.9	1.4 - 9.1	2.1 - 46.5
5	6 h	2.3 - 23.2	1.4 - 17.3	1.5 - 10.4	2.4 - 61.8
10	10 min	1.3 - 18.5	1.5 - 31.4	1.7 - 24.2	1.2 - 24.1
10	30 min	2.1 - 41.2	2.6 - 36.0	3.3 - 21.1	2.2 - 70.1
10	1 h	3.2 - 51.8	2.9 - 43.7	2.2 - 35.6	3.0 - 113.7
10	3 h	3.4 - 36.6	1.8 - 21.1	1.6 - 16.2	2.9 - 63.4
10	6 h	3.0 - 41.1	1.5 - 25.9	1.4 - 12.4	3.7 - 144.1
20	10 min	1.2 - 22.2	1.6 - 25.0	2.1 - 29.3	1.3 - 32.6
20	30 min	2.6 - 71.4	3.4 - 35.9	4.7 - 33.6	2.3 - 79.6
20	1 h	3.6 - 91.6	2.8 - 70.2	2.8 - 37.1	4.8 - 122.0
20	3 h	3.7 - 48.8	1.9 - 38.1	1.9 - 33.2	3.7 - 113.7
20	6 h	4.0 - 63.5	1.6 - 38.6	1.6 - 17.8	4.3 - 122.4
50	10 min	1.2 - 21.6	2.0 - 19.2	2.7 - 31.7	1.3 - 53.8
50	30 min	3.2 - 92.0	6.0 - 82.2	5.9 - 60.7	3.4 - 212.4
50	1 h	5.0 - 118.6	4.5 - 86.4	3.2 - 87.6	6.3 - 272.7
50	3 h	5.3 - 92.0	2.1 - 118.4	2.0 - 83.0	5.3 - 142.9
50	6 h	5.6 - 92.0	1.8 - 69.7	1.9 - 27.7	7.1 - 381.7
100	10 min	1.3 - 22.4	2.5 - 34.0	3.5 - 24.6	1.4 - 51.6
100	30 min	4.3 - 119.4	7.9 - 144.3	7.4 - 119.9	3.5 - 221.4
100	1 h	6.1 - 118.6	4.7 - 114.4	3.6 - 146.5	8.0 - 381.7
100	3 h	7.4 - 118.6	2.2 - 262.9	2.0 - 140.6	6.9 - 146.7
100	6 h	8.1 - 119.4	2.0 - 84.6	1.9 - 32.1	9.1 - 533.7
200	10 min	1.3 - 24.5	3.0 - 38.0	3.8 - 43.1	1.5 - 107.1
200	30 min	4.1 - 122.6	11.1 - 253.1	9.3 - 202.0	4.6 - 381.7
200	1 h	6.1 - 119.4	4.8 - 188.8	3.9 - 330.7	10.6 - 531.1
200	3 h	7.8 - 119.4	2.7 - 735.6	2.2 - 318.6	9.2 - 212.7
200	6 h	8.3 - 119.4	2.3 - 84.6	1.9 - 29.7	11.2 - 780.0